Cellular and Molecular Life Sciences (2024) 81:348
https://doi.org/10.1007/s00018-024-05355-4

ORIGINAL ARTICLE

Rhythms in lipid droplet content driven by a metabolic oscillator are conserved throughout evolution

Paula M. Wagner[1,2] · Mauricio A. Salgado[1,2] · Ornella Turani[3] · Santiago J. Fornasier[1,2] · Gabriela A. Salvador[3] · Andrea M. Smania[1,2] · Cecilia Bouzat[3] · Mario E. Guido[1,2]

Received: 4 March 2024 / Revised: 2 July 2024 / Accepted: 8 July 2024

Abstract

The biological clock in eukaryotes controls daily rhythms in physiology and behavior. It displays a complex organization that involves the molecular transcriptional clock and the redox oscillator which may coordinately work to control cellular rhythms. The redox oscillator has emerged very early in evolution in adaptation to the environmental changes in O_2 levels and has been shown to regulate daily rhythms in glycerolipid (GL) metabolism in different eukaryotic cells. GLs are key components of lipid droplets (LDs), intracellular storage organelles, present in all living organisms, and essential for energy and lipid homeostasis regulation and survival; however, the cell bioenergetics status is not constant across time and depends on energy demands. Thus, the formation and degradation of LDs may reflect a time-dependent process following energy requirements. This work investigated the presence of metabolic rhythms in LD content along evolution by studying prokaryotic and eukaryotic cells and organisms. We found sustained temporal oscillations in LD content in *Pseudomonas aeruginosa* bacteria and *Caenorhabditis elegans* synchronized by temperature cycles, in serum-shock synchronized human embryonic kidney cells (HEK 293 cells) and brain tumor cells (T98G and GL26) after a dexamethasone pulse. Moreover, in synchronized T98G cells, LD oscillations were altered by glycogen synthase kinase-3 (GSK-3) inhibition that affects the cytosolic activity of the metabolic oscillator or by knocking down LIPIN-1, a key GL synthesizing enzyme. Overall, our findings reveal the existence of metabolic oscillations in terms of LD content highly conserved across evolutionary scales notwithstanding variations in complexity, regulation, and cell organization.

Graphical abstract

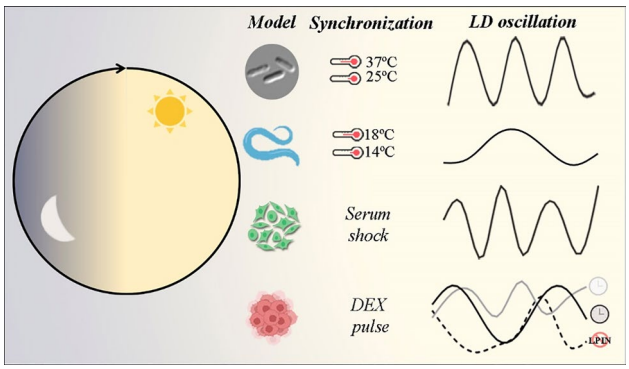

Keywords Metabolic oscillator · Lipid droplets · Biological rhythms · Evolution · Bioenergetics

Paula M. Wagner, Mauricio A. Salgado and Ornella Turani have been contributed equally to this work.

Extended author information available on the last page of the article

Published online: 13 August 2024

Introduction

The circadian timing system coordinates a plethora of physiological and behavioral rhythms in all vertebrates in a tight mechanism of environmental adaptation to the 24-h light/dark cycles [1]. The central clock is located in the suprachiasmatic nucleus of the anterior hypothalamus and is daily synchronized by ambient lighting through direct retinal projections from intrinsically photosensitive retinal ganglion cells (reviewed in [2]). The central clock coordinates numerous peripheral clocks in most organs and tissues, even in individual cells. Although the light/dark cycles are the main and strongest synchronizer of the circadian system, feeding and fasting schedules, locomotor activity, and temperature are important synchronizing cues [2–5]. At the transcriptional level, the circadian clock comprises a set of transcription factors operating through a transcription-translation feedback loop (TTFL) that involves positive elements, such as CLOCK, BMAL1, and NPAS2, and negative elements, such as Periods (PER 1, 2, 3) and Cryptochromes (CRY 1, 2). The molecular clock regulates clock- and clock-controlled gene (CCG) expression along the 24-h cycle through an E-box sequence in clock genes and CCG promoters. In addition, a second and interconnected loop participates in the control of clock gene expression that implies the nuclear receptors for the retinoic acid Rev-Erbs and the Retinoid-related orphan receptors (RORs) that operate on the ROR element (RORE) as negative and positive elements respectively, and mainly connecting the molecular clock with the cellular metabolism (reviewed in [4, 6]). At the cellular level, the biological clock comprises the molecular transcriptional clock (TTFL) and the metabolic/redox oscillator that may work together in a coordinated manner to control cellular rhythms (reviewed in [3, 7–10]). Studies in *Arabidopsis thaliana*, *Drosophila melanogaster*, and mammals showed that rhythms in small signaling molecules, primarily presented as "output" have a central role within the circadian pacemaker. Thus, clock outputs can constitute inputs to subsequent cycles and become indistinguishable from a core mechanism. Hastings et al. (2008) introduced the term "cytoscillator" or cytoplasmic oscillator to refer to circadian cytosolic signals such as cAMP and Ca^{2+}−dependent kinases, casein kinases, C-Jun amino-terminal kinases, ras-dependent (MAP) kinases and their various downstream effectors and modulators (e.g. Epac, GSK3β, phosphodiesterases, protein phosphatases) (reviewed in [10]). Remarkably, peroxirredoxin oxidation cycles are highly conserved through evolution in all kingdoms of life, even in transcription absence as observed in enucleated cells [8, 11]. Evidence for the autonomous function of the cytosolic components comes from studies in *Cry*-null SCN [12], *Bmal*1-null SCN [13], and CRY knockout mice [14] models that reported periodicity upon the activity and stability of PER2, suggesting that these findings entail an underlying, evolutionarily conserved post-translational timekeeping mechanism taking place in the cellular cytoplasm. This mechanism involves the activity of the casein kinase 1 δ/ϵ (CK1δ/ϵ) and the glycogen synthase kinase 3 (GSK-3) and determines the pace of the cellular circadian clock in eukaryotes through post-translational modifications of clock proteins [14]. Metabolic oscillations have been observed in different cell types and organisms from retinal neurons in birds to fibroblasts and liver cells in mice as indexed by daily rhythms in glycerolipid (GL), particularly glycerophospholipid (GPL) metabolism (reviewed in [3]). Moreover, sustained metabolic oscillations have also been reported in diverse synchronized tumor cells such as the human glioblastoma multiform-derived T98G cells, A530 cells from murine gliomas, and human hepatocarcinoma-derived HepG2 cells [15–17] with periods in the circadian and ultradian ranges. Remarkably, most metabolic rhythms were observed in synchronized cells by dexamethasone (DEX) pulses or a serum shock and were severely affected when the clock gene *Bmal1* was knocked down [15, 17].

Lipid droplets (LDs) are specialized intracellular organelles that play diverse functions such as energy stores from bacteria to man [18, 19]. They are composed of a core with neutral lipids, mainly triglycerides (TAGs), and cholesterol esters, and are surrounded by a monolayer of GPLs and specific proteins. Notably, in eukaryotic cells, LD biogenesis and degradation, together with their organelle interactions, are strongly coupled to cellular metabolism and critical in regulating the levels of toxic lipid species. Facilitating the coordination and communication between different organelles, LDs act as vital hubs of cellular metabolism [19]. The most predominant features of LDs are their heterogeneity and diversity. LD number, size, and composition vary widely among cells even within the same cell under different conditions [18, 20–23]. LD growth and degradation are controlled by enzymes that promote TAG synthesis and hydrolysis, respectively. In this respect, the phosphatidate (PA) phosphatase 1, or LIPIN-1, is a key enzyme in the biosynthetic pathway of more complex GPLs and TAGs from PA. Strikingly, the rapid and dramatic changes in LD size, number, and distribution occur in response to cellular metabolism and nutrient availability. In this connection, it has been shown that the BMAL1: CLOCK transcriptional complex activates TAG hydrolysis through the upregulation of TAG lipase and hormone-sensitive lipase, thus providing evidence about the crucial role of the core molecular clock in modulating LD metabolism across the circadian cycle [24].

As observed for the rhythms in peroxiredoxins along evolution, cells needed to develop a precise temporal mechanism to control the increase in ROS levels for detoxification. For every cell, the energy requirement is essential for survival and displaying several vital tasks and homeostasis regulation; however, the bioenergetics status varies along the 24-h cycle and depends on the nutrient´s availability and energy demands. In this regard, the dynamic formation and degradation of each LD within the cell may represent a time-regulated process adapting to the fluctuations in energy requirements. In this context, we tested the hypothesis that metabolic oscillations in LD content are conserved across various phylogenetic kingdoms. For this, we examined LD rhythmic patterns in different cellular and organism models, including bacteria, invertebrates, and embryonic and tumor human cells.

Materials and methods

Cell cultures and synchronization conditions

Pseudomonas bacteria

The *Pseudomonas aeruginosa* HEX-1 T strain, isolated from soil and previously characterized [25], was routinely subcultured on Luria–Bertani (LB) agar medium from stocks stored at −80 °C. For synchronization, bacteria were cultured in sterile Erlenmeyer flasks shielded from light with 20 ml of LB medium under the following conditions: 12 h at 37 °C followed by 12 h at 25 °C for 3 days. Non-synchronized cultures were kept at a constant temperature of 37ºC. Subcultures were performed every 24 h using the previous day's culture as the inoculum to refresh the culture medium and prevent the system from entering the death phase. Samples were collected every 4-h intervals after synchronization for 36 h.

Caenorhabditis elegans

Nematodes were obtained from the *Caenorhabditis* Genetics Center, supported by the National Institutes of Health—Office of Research Infrastructure Programs (P40 OD010440). The strain used was N2, recognized as the reference wild-type strain. Worms were maintained at 18–25 °C using freshly prepared Nematode Growth Medium (NGM) Petri dishes spread with *Escherichia coli* (OP50) as a source of food [26, 27]. The endogenous circadian clock was synchronized by temperature according to the protocol reported before [28]. For this, gravid adult wild-type worms were treated with a hypochlorite bleach solution to obtain the eggs, which were maintained in distilled water under rotation overnight to obtain L1 larvae. For the synchronization, a population of wild-type L1 larvae was entrained until the young adult stage through 12 h:12 h temperature cycles (14 °C–18 °C) in constant darkness. After the synchronization, when worms reached the young adult stage, the temperature was maintained constant at 14 °C, and worms were fixed every 6-h interval for 36 h. Two independent replicate experiments were performed, and 3 to 5 worms of each experiment were evaluated for each time point post-synchronization. As non-synchronized controls, wild-type L1 larvae were maintained at a constant temperature (14 ºC) until the young adult stage, and samples were collected as described above. Worms were fixed with isopropanol 60% for 3 min at room temperature, washed 3 times with phosphate-buffered saline (PBS), and centrifuged at 2000 rpm for 2 min. The samples of fixed worms in PBS were maintained at 4 °C until staining.

HEK 293 cells The HEK-293 cell line (human embryonic kidney 293 lineage) (ATCC Cat# PTA-4488, RRID: CVCL_0045) was cultured in Dulbecco's Modified Eagle Medium (DMEM), (Gibco, BRL, Invitrogen) supplemented with 10% (v/v) fetal bovine serum (FBS) in a CO_2 incubator at 37 °C. The cell cultures were synchronized by a 50% FBS shock in DMEM culture medium for 1 h in a CO_2 incubator at 37 °C [29]. Samples were collected every 4-h intervals post-synchronization for 36 h.

Tumor cells

T98G cells are derived from a human glioblastoma (GBM) (ATCC, Cat. No. CRl-1690, RRUD: CVCL0556). The GL26 cell line is derived from a murine GBM and was gently donated by Dr. Marianela Candolfi (Instituto de Investigaciones Biomédicas, Facultad de Medicina, Universidad de Buenos Aires, Argentina). Cell cultures were grown in DMEM supplemented with 10% FBS according to [15] at 37 ºC and 5% CO_2. Cell cultures were synchronized with dexamethasone (100 nM, DEX) for 1 h at 37ºC. Then, cells were washed with PBS to remove DEX and cultures were maintained in DMEM supplemented with 5% FBS. Samples were collected every 6-h intervals post-synchronization for 48 h.

Glycogen synthase kinase-3 inhibitor treatment on T98G cells

T98G cells were treated with CHIR99021, a glycogen synthase kinase 3 inhibitor (GSK-3 Inhibitor XVI, Santa Cruz) at a final concentration of 8.6 µM for 24 h at 37ºC. CHIR99021 stock solutions were resuspended in DMSO at a final concentration of 20 mM, and the maximum volume of DMSO in cell cultures was < 0.05%.

Lipin-1 knock-down

Lipin-1 expression was disrupted in T98G cells using the CRISPR/Cas9 genomic editing tool according to [15, 16]. We designed single guide RNAs (sgRNA) specifically targeting exon 5 of the human *Lipin*-1 gene and subcloned it into the PX459 vector (Addgene) to obtain the PX459-*Lipin*-1 plasmid. The primer sequence corresponding to the top and bottom sgRNA was 5´ACCACTCTCTAT CCGAATTA3´ and 5´TAATTCGGATAGAGAGTG GT3´, respectively. GBM cultures were transfected with Lipofectamine 2000 (Invitrogen) and selected with puromycin (1 µg/mL) for 5 days. T98G denoted as F4 *Lipin*-1 knockdown (KD) cells correspond to one clone isolated from the pool of puromycin selected-T98G cells. The disruption of *Lipin*-1 gene expression was checked by the polymerase chain reaction (PCR) and western blot (WB).

Lipid droplet identification

Pseudomonas bacteria

After synchronization, the cultures were maintained at a constant temperature (37 °C), and duplicate samples were collected every 4 h for 36 h. Immediately after extraction from each flask at each time point, the optical density (OD) at 600 nm was measured using either the PG instruments T60UV-Visible Spectrophotometer or the Shimadzu biospec-mini spectrophotometers. Subsequently, aliquots were stained with Sudan Black B (SB) dye following procedures described in [30, 31] with minor modifications. The absorbance at 600 nm of these stained aliquots was then determined. The ratio between the post-staining OD value (OD_f) and the OD before staining (OD_i) was used to standardize the lipid content. Additionally, images were captured before and after staining using the Olympus FV1000 microscope to confirm the dye's penetration into the bacteria.

Caenorhabditis elegans

LDs were stained using Oil Red, a dye-based method for neutral lipid staining validated as an accurate assessment for major fat storage in *C. elegans* [32]. Worms from all time points of each experiment were stained together with Oil Red 0.3% (100 µl per condition) during 1 h in rotation. Oil Red was prepared and filtered before being used. After the staining, the worms were washed with PBS. The images of LDs were obtained by an LSM 900 (Zeiss) confocal microscope with an Airyscan 2 module. For each worm, a general image in 10X was obtained and after that, a series of images in 40X were obtained for LD quantification. Confocal microscopy images were generated in a single plane where the staining intensity was higher. In *C. elegans*, the intestine functions as the fat metabolic organ and lipids accumulate mainly in hypodermal and intestinal cells [33]. Hence, images were taken from the posterior region of the pharyngeal terminal bulb to the anus. ImageJ software (RRID: SCR_002285) carried out the average size, percentage area, and number quantification of LDs. The LD number and percentage area were normalized by the selected area of the worm.

HEK 293 cells

After synchronization, samples in duplicate were collected every 4 h for 36 h. The samples were washed with PBS at room temperature and fixed with 3% (w/v) paraformaldehyde (PFA) solution containing 4% (w/v) sucrose, for 15 min at 4 °C. The fixed samples were washed with PBS and incubated with Nile Red (NR, 0,05 µg/ml) and DAPI (3 µM) in PBS for 10 min. Then, coverslips were washed with PBS three times at room temperature for 5 min in darkness. To visualize LDs in HEK293 cells, the confocal microscopes Olympus FV1000 (with a PlanApo N 60X objective, numerical aperture 1.42) and FV300 were used. They were equipped with a dichroic mirror filter set at 405/488/543 nm and lasers at 405 nm and 543 nm to excite DAPI and Nile Red, respectively. Three fields were photographed per coverslip, with a variable number of cells. A Z-stack projection was performed for each field since LDs were dispersed across multiple planes. The photographs were analyzed using the ImageJ software (RRID: SCR_002285). The number of LDs was normalized by the number of nuclei to obtain an approximate average of the LD number per cell.

Tumor cells

$1*10^4$ T98G cells, F4 *Lipin*-1 KD T98G cultures, or GL26 cells were seeded in coverslips and synchronized with 100 nM DEX for 1 h at 37ºC. Culture cells were maintained in DMEM supplemented with 5% SFB. After DEX synchronization (t_0), cells were collected in duplicate every 6 h for 48 h. For LD staining, cells were fixed with 4% PFA for 15 min and washed twice with PBS according to [17, 34]. Then, T98G cell coverslips were incubated with BODIPY dye (Sigma cat#790389, maximum excitation/emission wavelength: 493/503 nm) at a final concentration of 2 µM for 30 min protected from light. GL26 cell coverslips were incubated with BODIPY dye at a final concentration of 75 µM for 1 h protected from light. Coverslips were washed two to four times with PBS and visualized by confocal microscopy at 60X objective (FV1200; Olympus). Cellular nuclei were visualized by DAPI staining (T98G cells) or Hoechst staining (GL26 cells). ImageJ software (RRID: SCR_002285) was used to determine the average size, percentage area, and number of LDs. The number and percentage area were normalized by the number of

cells in each image. For LD determination of CHIR99021-treated cells, cultures were incubated with CHIR99021 (8.6 µM, GSK-3 Inhibitor XVI, Santa Cruz) for 24 h before synchronization and then analyzed as described above.

Statistical and Periodic Analysis

Statistical analysis involved one-way ANOVA to test the time effects on LD parameters with Tukey's multiple comparisons test, or the Kruskal Wallis (K-W) analysis with Dunn's multiple comparisons test, when the normality of residuals was infringed. In all cases, significance was considered at $p < 0.05$. To analyze significant differences in LD number between T98G control and CHIR-99021-treated cells or T98G control and F4 *Lipin*-1 KD cultures, a two-way ANOVA was performed to test the effect of treatment/cell type and time post-synchronization.

Experimental data was analyzed against three alternative rhythmicity algorithms to test its periodicity. Both ARSER (ARS) and JTK_CYCLE (JTK) methods implemented by the Metacycle package [35] and RAIN [36] algorithm were performed in R (4.0.3). It is important to evaluate periodicity in time-series data against different algorithms due to some of them performing better on experimental data with higher levels of noise, non-24-h periods, or various sampling conditions. In this case, both the ARS and JTK_CYCLE detect sinusoidal waveforms whereas the RAIN algorithm can detect oscillations with narrow peaks or troughs [37]. LD variations in the different models were graphed using the amplitude, phase, and period values of the ARS algorithm to model the time series using harmonic regression ((y = cos (2 × pi × (time—phase)/period) × amplitude + mean).

Results

To ascertain metabolic oscillations across evolution, we analyzed the rhythmic patterns of LD content following specific synchronization stimuli in prokaryotic (*Pseudomonas aeruginosa*) and invertebrate (*C. elegans*) models, as well as in human cells, including human embryonic kidney cells (HEK-293) and mammalian tumor glioma cells (human T98G and murine GL26).

Lipid droplet oscillations in prokaryotes

To investigate lipid content oscillatory patterns in prokaryotes, we employed the *Pseudomonas aeruginosa* HEX-1 T strain, a chemotrophic bacterium that causes opportunistic infections in diverse hosts. Bacteria cultures underwent synchronization through temperature cycles spanning 3 days, with samples collected at 4-h intervals post-synchronization. Subsequently, bacteria were stained with Sudan Black B (Fig. 1a) to quantify lipid content (see Materials and Methods for detailed protocols). Results showed a significant temporal effect on lipid content in synchronized bacteria over a 36 h period ($p < 0.0001$ by Kruskal–Wallis test), with pronounced lipid staining at 4, 8, 16, 20, and 28 h post-synchronization, and reduced levels at 0, 12, 24, 32, and 36 h. Upon fitting the experimental data to a periodic function using the ARS and JTK_CYCLE methods from the Metacycle package, a distinct 12-h cycle emerged (Fig. 1c; Table 1, Suppl. Table 1). In contrast, non-synchronized bacteria cultures exhibited a weak and damped oscillation (Suppl. Figure 1) in lipid content but without a 12-h significant periodicity when the experimental data was adjusted to a periodic curve using the ARS method or the JTK_CYCLE algorithm (Fig. 1b).

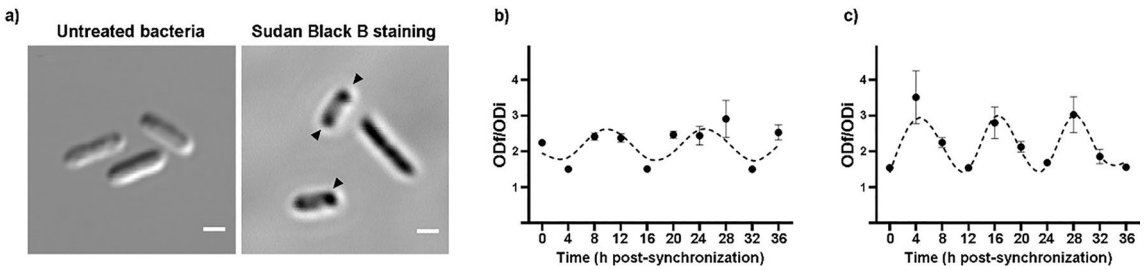

Fig. 1 Lipid droplet oscillations in *Pseudomonas aeruginosa* HEX 1 T. **a** Representative images of confocal microscopy of untreated bacteria (left) and cultures after Sudan Black B staining (right). The arrows indicate stained lipid accumulations Scale bar = 1 µm. **b** Non-periodic variation was observed in LD content in non-synchronized cultures. **c** Temperature-synchronized bacteria evidenced a significant oscillation with a period of 12 h ($r^2 = 0{,}967$, dashed curve) using the ARS method. OD_f/OD_i is the ratio of final optical density (OD_f) to initial optical density (OD_i). The black dots represent the mean of three independent experiments performed in duplicates ± SD

Table 1 Lipid droplet number oscillations in different models

Model	Cell type/organism	Period (h)	p-value	r^2
Pseudomonas	Bacteria	12	0.0007	0.967
C. elegans	Nematode	29	0.0091	0.99
HEK293 cells	Human embryonic kidney cells	10	0.003	0.85
T98G cells	Human glioblastoma cell line	29	0.002	0.99
CHIR-T98G cells	Human glioblastoma cell line treated with CHIR99022	16	0.02	0.96
LIPIN-1 KD-T98G cells	Human glioblastoma cell line knockdown for LIPIN-1	33	0.015	0.97
GL26 cells	Murine glioma cell line	29	4.8E-7	0.99

Periodic analysis of LD number variations in different models. MetaCycle analysis using the ARS method was performed to test periodic oscillations in LD number

p-value < 0.05 indicates a significant effect on the fit of the experimental data with respect to the theoretical curve. See methods for further details

Lipid droplet rhythms in an invertebrate model organism

Caenorhabditis elegans is a soil nematode extensively used as a model organism to perform studies related to genetics, developmental biology, fat metabolism, and circadian rhythms [38, 39]. It is an excellent animal model to study the regulation of fat accumulation and distribution [32]. Also, its transparent body facilitates qualitative assessment of lipid distribution among different tissues [40]. We examined LD content variations in wild-type nematodes to investigate possible metabolic oscillations in this invertebrate model. Worms were either synchronized by temperature cycles (12 h (14 °C): 12 h (18 °C)) or maintained at constant temperature (14 °C), in constant darkness, from L1 larval to the young adult stages. After reaching the young adult stage (about 3–4 days), the nematodes were maintained at a constant temperature (14 °C) and samples were fixed at different times along 36 h for both experimental conditions. In Oil Red stained worms, the LD quantification was made from the posterior region of the pharyngeal terminal bulb to the anus. At the longer times evaluated (> 30 h), worms contained eggs which were stained by Oil Red as reported in the literature [41]. However, the Oil Red signal from eggs was not detected in the single planes selected for confocal images. In synchronized worms, we found a significant time-dependent effect on LD number and percentage area examined by confocal microscopy ($p < 0.0001$ by one-way ANOVA, $p < 0.002$ by Kruskal–Wallis test, respectively) (Fig. 2, Table 1). No significant variations were observed in the average size of LDs in these worms. The lowest levels for both parameters were achieved at 30 and 36 h after synchronization (Suppl. Table 2). Experimental data was analyzed against different algorithms to carry out the periodic adjustment. A significant period of 24–29 h was detected when the 3 parameters tested (LD number, percentage area, and average size) were adjusted to a periodic function using the ARS method. A longer period (36 h) was evidenced by the RAIN method only in the number and percentage area of LDs (Fig. 2, Table 1, Suppl. Table 1).

On the other hand, a slight, but statistically significant time-dependent effect on the percentage area ($p < 0.043$ by Kruskal–Wallis test) and average size ($p < 0.041$ by one-way ANOVA) was found in non-synchronized worms kept at constant temperature (Fig. 2). Notably, and in contrast to the observations in temperature-synchronized worms, no periodic fit was observed when the experimental data of LD number and percentage area of non-synchronized worms were analyzed using the RAIN algorithm (Suppl. Figure 2, Suppl. Table 1 and 2).

Lipid droplet rhythms in vertebrate models

Embryonic HEK-293 cells

Having observed LD oscillations with different periods in synchronized prokaryotes and the invertebrate model, we extended these studies to identify any potential temporal variation in lipid accumulation in eukaryotic cells from diverse origins. For this, in the first series of studies, HEK-293 cells were synchronized by a serum shock, collected every 4 h post-synchronization over 36 h, and stained with Nile Red to identify LDs. A significant effect of time was observed in LD content along the 36 h post synchronization tested ($p < 0.01$ by Kruskal Wallis test) (Suppl. Table 2), showing the highest values at 8, 16, and 36 h post-synchronization. Remarkably, the number of LD per cell exhibited a clear rhythmicity with a period near 10 or 8 h when the experimental data was adjusted to a periodic function using the ARS or the JTK_CYCLE method, respectively (Fig. 3, Table 1, Suppl. Table 2).

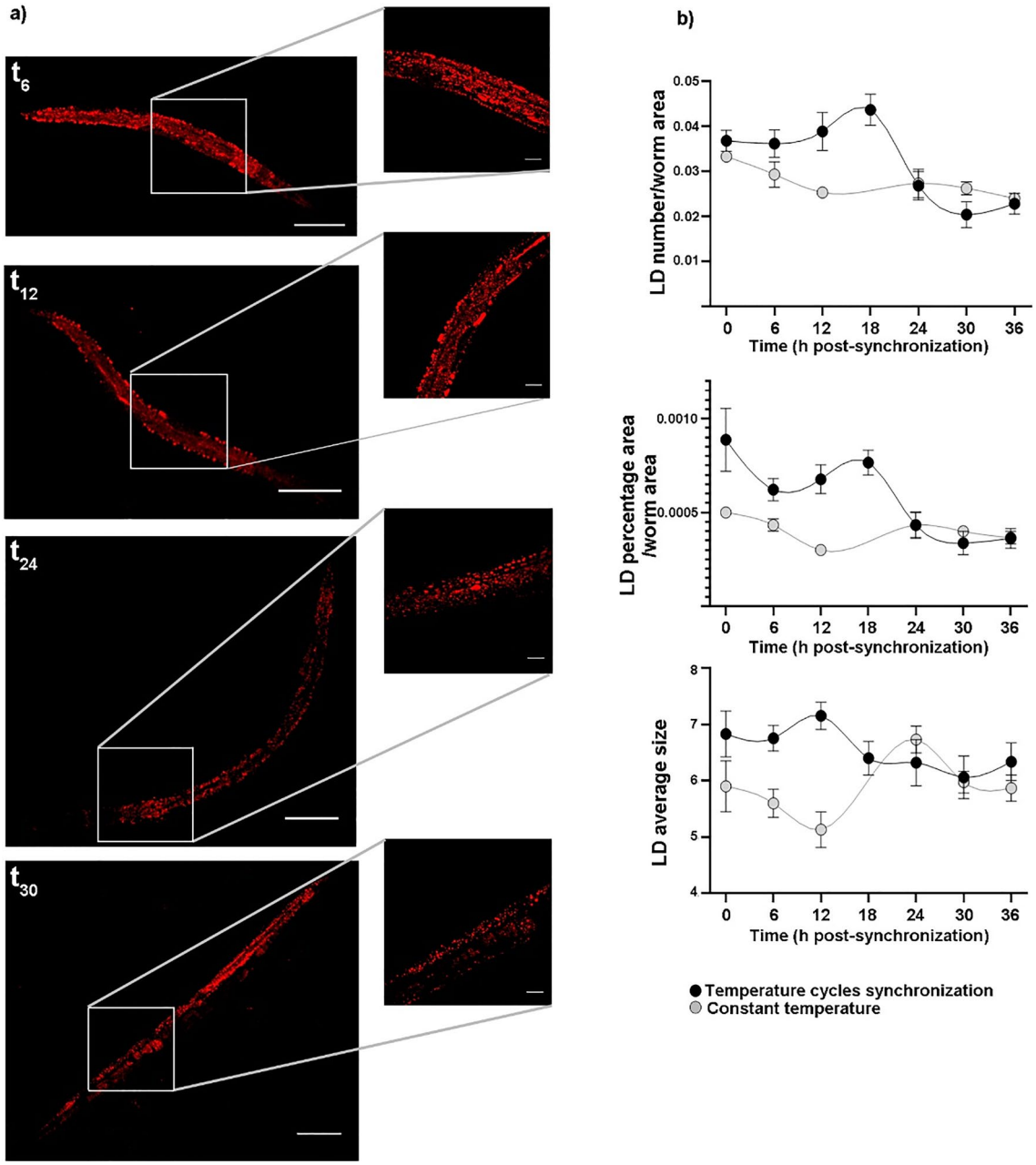

Fig. 2 Lipid droplet parameters (average size, number, and % area) in *C. elegans*. The L1 larvae population was synchronized by temperature cycles (black circles) or maintained at constant temperature (gray circles) and fixed at each 6-h intervals for 36 h. **a** Representative image of adult worms fixed at t_6, t_{12}, t_{24}, and t_{30} h after synchronization and stained with Oil Red (left column, scale bar = 100 µm). LD accumulation is shown in red. Further magnified in the insets are on the right column, scale bar = 20 µm. The insets correspond to the anterior middle region of the worm. **b** Periodic analysis of LD parameters in synchronized worms (black circles) using the ARS method indicated a significant period of 29, 24, and 28 h in terms of the number, percentage area, and average size, respectively (dashed curve). The black dots represent the mean of two independent experiments (n = 3–8 worms analyzed per experiment) ± SEM

Tumor cells

Once we evidenced LD rhythms in a human embryonic cell line, we evaluated if this metabolic periodicity also occurs in brain tumor cells. Previous results from our laboratory evidenced an intrinsic metabolic clock that functions in glioblastoma tumor cells, controlling diverse metabolic pathways and highlighting differential states of tumor suitability for more efficient time-dependent chemotherapy [15, 42]. Here, we evaluated if these immortalized tumor cells

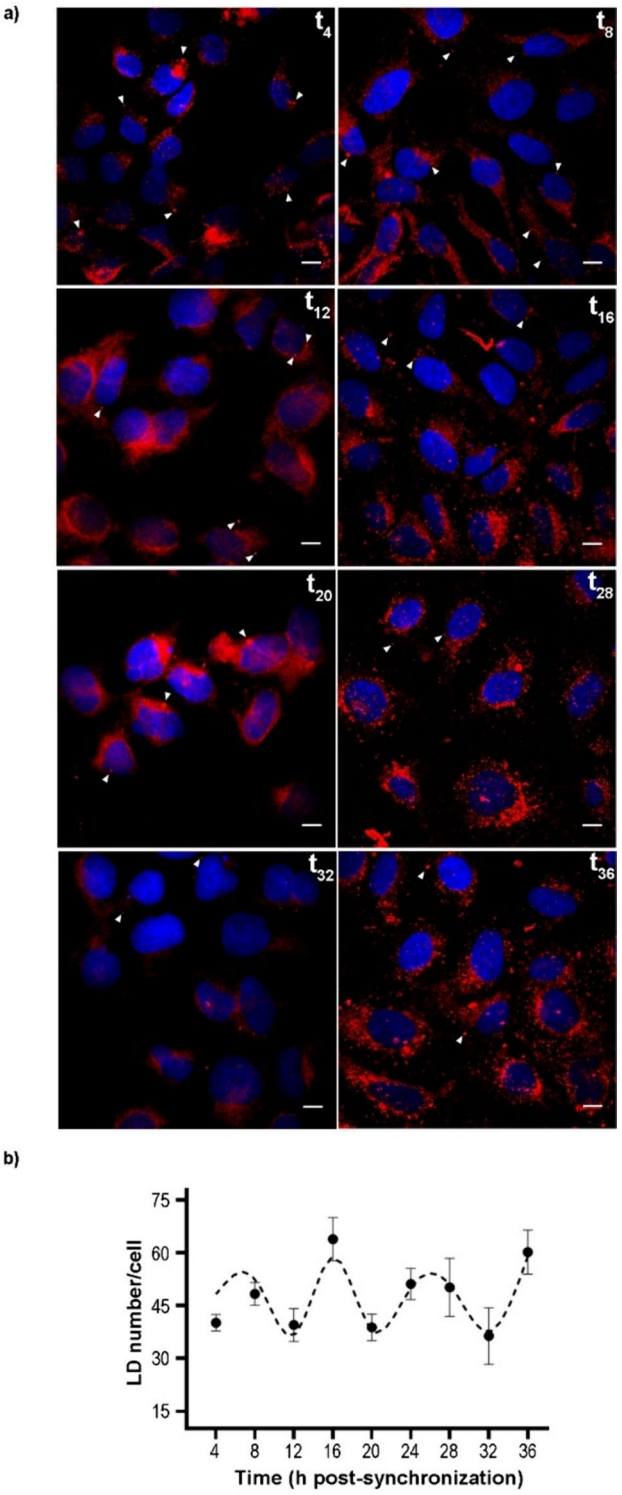

Fig. 3 Lipid droplet number oscillation HEK293 cells. **a** Representative confocal microscopy images of LDs in HEK293 cells across time. Nile Red and nuclei staining are shown in red and blue, respectively. Scale bar = 10 µm. **b** Periodic analysis of LD number per cell using the ARS method indicated a significant period of 10 h ($r^2 = 0.851$, dashed curve). The black dots represent the mean of three independent experiments performed in duplicates ± SEM

exhibit rhythms on different LD parameters including number, size, and percentage area. For this, synchronized T98G cells derived from a human glioblastoma were fixed at different times post-synchronization and stained with BODIPY dye. The results clearly showed a significant time-dependent effect on LD number and percentage area ($p < 0.001$ and $p < 0.01$ by Kruskal–Wallis test, respectively) (Suppl. Table 2) displaying high LD levels at 12 and 36–40 h and low levels at 24–30 h after DEX synchronization (Fig. 4). To elucidate the periodicity for these oscillations, experimental data was analyzed against three alternative algorithms. Results from the ARS and JTK method integrated into the Metacycle package showed periodic oscillations of 28–30 h for the LD number and percentage area parameters whereas the average size evidenced a significantly shorter period of 17–18 h. Moreover, similar results for LD number and percentage area were obtained when the oscillation observed was fitted to a periodic function using the RAIN algorithm which can detect asymmetric circadian oscillations (Fig. 4, Table 1, Suppl. Table 1). When these observations were extended to another glioma cell model, metabolic oscillations in different parameters of LDs were also found. In synchronized GL26 murine GBM cells collected at different times post-synchronization along 48 h, we found a significant effect of time on LD number and average size ($p \leq 0.02$ by one-way ANOVA) (Suppl. Table 2). A significant oscillation with a 29 h-period was seen for the LD number by the ARS method. However, longer periods of 42 and 48 h were shown by the JTK and the RAIN algorithms for the LD number and average size, respectively (Suppl. Table 1Table 1, Suppl. Figure 3). In addition, a significant rhythm with a period of 20–24 h was observed for the LD percentage area when the experimental data was evaluated both with the ARS and the RAIN algorithms (Suppl. Figure 3, Suppl. Table 1).

Pharmacological modulation of the circadian clock: Effect of the treatment with the GSK-3 inhibitor (CHIR99021) on T98G LD rhythms

To establish if there is an interplay between LD oscillations and the cytoscillator on the glioblastoma cell line, we next examined whether the pharmacological modulation of the cytosolic kinases could affect the periodic oscillations observed using the GSK-3 inhibitor (CHIR99021). For this purpose, T98G cells were treated with the GSK-3 inhibitor (CHIR99021, 8.6 µM for 24 h) before DEX synchronization (Fig. 4). Interestingly, CHIR99021-treated cells exhibited a significant effect of time on LD number, percentage area, and average size ($p < 0.01$ by the Kruskal–Wallis test, $p < 0.0001$ by the Kruskal–Wallis test, and $p < 0.01$ by one-way ANOVA test, respectively) (Suppl. Table 2). Remarkably, the

content of LDs, assessed across the three parameters, exhibited a pronounced decline approximately 36 h and beyond following synchronization with a reduced amplitude as compared to the vehicle-treated cells, likely suggesting the loss of rhythmicity at longer times of cell culture treatment. A two-way ANOVA with the factors of time and pharmacological treatment revealed a significant effect of time ($p < 0.0123$) and of interaction between time and treatment ($p < 0.0009$) but not of treatment alone ($p = 0.1$, ns) for the LD number. The pairwise comparisons by Bonferronis´s test clearly showed that levels of LDs from CHIR99021-treated cells at 24 h post-DEX synchronization significantly differed from the control samples (Fig. 4b). Regarding LD oscillations after GSK-3 inhibition, the ARS method showed significantly shorter periods (16–17 h) and the JTK algorithm revealed the loss of rhythmicity in the circadian range compared to control cells in terms of LD number and percentage area parameters. In parallel, RAIN results also showed no significant periods in the circadian range displaying 48 h for LD percentage area and number. In line with this, the average size of LDs displayed a rhythm of 42 h by the ARS method and no significant oscillations were identified by the JTK or RAIN algorithms (Fig. 4, Table 1, Suppl. Table 1).

Metabolic disruption: Effect of LPIN knockdown on T98G LD rhythms

To examine whether the expression of key regulatory lipid synthesizing enzymes could alter metabolic oscillations in glioblastoma cells, we evaluate LD rhythms after LIPIN-1 disruption, a key enzyme in GL synthesis. Once we confirmed a significant reduction in LPIN expression on transfected T98G cells (Suppl. Figure 4), LDs were stained with BODIPY on synchronized cell cultures. Results evidenced a significant effect of time in LD average size ($p < 0.025$ by one-way ANOVA). No significant differences were observed throughout the times tested in LD number and percentage area (Suppl. Table 2). A two-way ANOVA with the factors of time and cell type revealed a significant effect of time ($p < 0.0246$), cell type ($p < 0.0195$), and interaction ($p < 0.0144$) for the LD number. The pairwise comparisons by Bonferronis´s test clearly showed that levels of LD at 18 h after synchronization for the LIPIN-1 KD cells significantly differed from the wild-type cells (Fig. 4c). For rhythmicity analysis, no significant periodic adjustment was observed in the LD percentage area or average size. Only the ARS method evidenced a significant oscillation in LD number with a period of 33 h. Absolute values were similar in LD number and percentage area of both groups. However, higher values in LD average size were observed in LIPIN-1 KD compared to control cells (Fig. 4, Table 1, Suppl. Table 1).

Discussion

All phyla across the life tree store fat in LD. The initial biochemical characterization of LD in the simplest organisms defines them as exclusive cell stores for energy; however, a deeper investigation in the last decades shed light on multifaceted roles in cell biology and physiology for LD [19, 43]. The expanded knowledge of LD functions defines them as a hub of metabolism and signaling balancing crucial mechanisms related to life and death. LDs maintain energy and redox homeostasis to protect cells from toxic lipid species during stress events. Since cellular compartmentalization is a key biological principle displayed throughout the different kingdoms of life, LDs offer an effective platform for biochemical processes related to metabolism and signaling [43–45]. Therefore, we tested the hypothesis that metabolic rhythms in LD content are conserved across different phylogenetic kingdoms. Next, we provided evidence of the changes observed in LD oscillatory patterns in tumor cells after pharmacological inhibition of the cytosolic kinase GSK-3 or genetic disruption of *Lipin*-1.

To investigate the existence of metabolic oscillations across different kingdoms of life, we initially examined metabolic variations in LD content within a prokaryotic model. Bacteria and archaea typically accumulate lipids in various forms, such as polymeric polyhydroxyalkanoates, TAG, and/or wax esters in the case of oleaginous bacteria [46–49]. Our analysis of temperature-synchronized *P. aeruginosa* cultures revealed a significant variation in the lipid content, with a distinct 12 h periodicity using three different algorithms (Table 1, Suppl. Table 1) and peak levels observed at 4, 16, and 28 h post-synchronization. Remarkably, non-synchronized cultures exhibited a weak oscillatory pattern but a non-significant 12-h rhythmic variation. Although previous studies have reported 24-h cycles in peroxiredoxin oxidation in bacteria [11], our findings represent the first evidence of metabolic oscillations related to lipid storage in *P. aeruginosa* within the ultradian range. Temperature serves as a crucial modulator of cellular physiology, influencing the regulation of gene and protein expression and behavior [50]. For instance, a thermosensory PAS domain was recently discovered in a protein from the *P. aeruginosa* strain PAO1, which regulates cellular levels of the ubiquitous bacterial second messenger c-di-GMP, exerting global effects on development and motility [51]. Recent studies have revealed that light/dark and temperature cycling during the growth of *P. aeruginosa* biofilms can impact respiratory activity and redox metabolism, thereby affecting the expression of genes encoding components

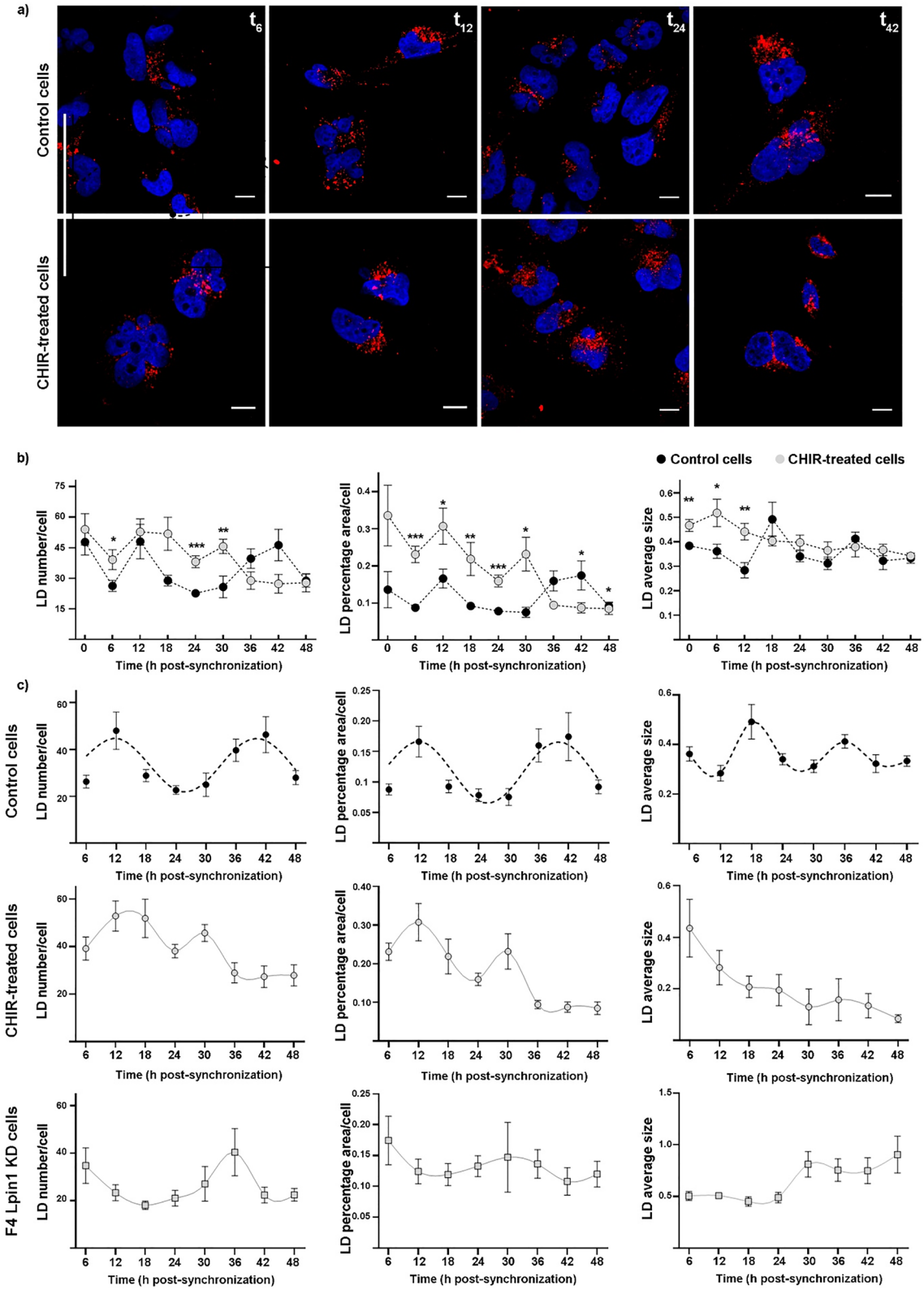
a)
Control cells
CHIR-treated cells
t6
t12
t24
t42
b)
Control cells
CHIR-treated cells
LD number/cell
LD percentage area/cell
LD average size
Time (h post-synchronization)
c)
Control cells
CHIR-treated cells
F4 Lpin1 KD cells
LD number/cell
LD percentage area/cell
LD average size
Time (h post-synchronization)

◂**Fig. 4** Lipid droplet parameters (average size, number, and percentage area) in T98G cells. T98G control or CHIR-treated cells were synchronized by a 1 h pulse of DEX (100 nM) and then collected at different times for LD assessment. **a** Representative microphotographs of LD staining across time in both conditions. BODIPY and nuclei staining are shown in red and blue, respectively. Scale bar = 10 µm. **b** Quantification of LD number, percentage area, and average size in control (black circles) and CHIR99021-treated cells (gray circles). Significant differences between experimental conditions were observed at certain times post-synchronization by unpaired t-test or Mann–Whitney test (* $p < 0.05$, ** $p < 0.001$, *** $p < 0.001$). **c** Periodic analysis of LD parameters using the ARS method indicated a significant period of 29, 28, and 17 h for control cells (black circles) in the number, percentage area, and average size parameters, respectively (dashed black periodic curve). On the contrary, CHIR99021-treated cultures (gray circles) evidenced significant periods of 17, 16, and 42 h in the LD number, percentage area, and average size parameters, respectively (full gray experimental curve). F4 *Lipin*-1 KD cultures (gray squares) revealed a significant oscillation of 33 h in terms of LD number; no significant variations were observed in the percentage area or average size of LD using the ARS algorithm (full gray experimental curve)

of the electron transport chain [52]. Hence, the observed temporal variations in lipid content within this bacterial species could be associated with cyclic alterations in storage lipid metabolism in response to temperature fluctuations.

Regarding lower animals, all metazoans accumulate TAG and/or cholesterol esters in their LDs; particularly for *C. elegans,* here used as an invertebrate model, it has been shown LD accumulation throughout the body cells with the highest concentration in the gut epithelium [38, 53]. In terms of circadian rhythms, *C. elegans* has been shown to display rhythms in locomotor activity, physiology, metabolism (abiotic and biotic stress tolerance, food and oxygen consumption), protein activity and regulation, and gene expression (reviewed in [54]). In line with the circadian rhythms described in *C. elegans* for different processes, we showed for the first time sustained rhythmicity in the number and percentage area of LDs, with periods fluctuating in the circadian range or longer from 24 to 29 h. The metabolic oscillations observed in LDs may reflect the daily requirement of lipids and energy for the nematode to complete its larval to adult transition and interaction with the environment, food availability, and higher locomotion activity at particular times. The multiple functions that can be buffered by lipids in LD variations observed in *C. elegans* could also be associated with a differential metabolic state for affording challenges such as responses to stress signals, defenses against pathogens, or buffering toxic lipid species. Once the metabolic oscillations in bacteria and *C. elegans* were described, we further investigated such oscillatory behavior in eukaryotic cells of mammals from three different models, a human embryonic kidney-derived (HEK-293) and a human and murine glioblastoma-derived (T98G, GL26) cell lines. HEK-293 cells kept in culture and synchronized by a brief serum shock display sustained oscillations in LD content with short periods in the ultradian range. These fluctuations in embryonic cells with this particular timing may reflect a differential activity of immature kidney cells or special requirements in lipid and energy for the early stages of kidney differentiation and development.

On the other side, and regarding tumor cells, we have taken into consideration the numerous LD functions in cancer, i.e. promoting tumor proliferation, driving epithelial-mesenchymal transition, mediating radio-resistance and chemo-resistance, maintaining cancer cell stemness, and avoiding immune destruction (reviewed in [55]. Because of this, we further investigated LD oscillations in glioblastoma cell lines. Previously, we reported significant rhythmicity in proliferative T98G cultures in the labeling of total ^{32}P-GPLs and individual GPL species, such as phosphatidylcholine (PC), with a period of 24 and 32 h, respectively, and a 24-h periodicity in the total LIPIN enzyme activity, evidencing a functional metabolic clock in glioblastoma cells [15]. Remarkably, LIPIN-1 dephosphorylates phosphatidic acid (PA) to diacylglycerol (DAG) to synthesize PC, phosphatidylethanolamine (PE), phosphatidylserine as well as TAGs (reviewed in [3]). In support of the previous evidence of a functional metabolic clock in tumor cells, we reported here periodic self-sustained oscillations of LD content in synchronized-T98G cultures with rhythms of 28–30 h for the number and percentage area, and of 17–18 h or longer for average size parameters. Additionally, we described oscillations in these LD parameters in synchronized GL26 cells, which display rhythms of 48 h for the average size, ≥ 29 h for the number, and 20–24 h for the LD percentage area. LDs also show periodic oscillations in hepatocellular carcinoma which was severely altered in terms of size and percentage area after *Bmal*1 disruption [17]. Strikingly, tumor cells from different origins and mammalian species display self-sustained rhythms in the content of LDs with periods ranging from the ultradian to circadian or longer.

The monolayer of GPLs is a critical factor for the stability and curvature of LDs and is expected to change depending on the physiological cellular state [56]. In fact, the cylindrically shaped characteristics of PC are crucial to LD stability, in contrast to the cone-shaped and negatively curved PE (reviewed in [19]). Circadian oscillations of choline kinase-α (Chok-α) expression and activity as well as in PC levels have been previously described in different models (reviewed in [3]) [57]. Therefore, the periodic oscillations of LDs described could be due in part to the circadian regulation of GPL and TAG metabolism at the lipid content, mRNA, and activity level of specific enzymes, likely including the Chok-α and LIPIN-1 axis as shown in HepG2 cells [17] together with a novel activity recently described for the Chok-α shown to promote LD lipolysis [58].

In the attempt to decipher the mechanisms involved in LD rhythms, we explored how the inhibition of GSK-3 affects these oscillations. We found metabolic alterations in T98G after the GSK-3 inhibition using the selective pharmacological inhibitor CHIR99021. Together with the casein kinase 1 δ/ϵ (CK1δ/ϵ), GSK-3 determines the speed of the cellular circadian clock in eukaryotes [10, 14, 59] by controlling the half-lives of clock proteins, even in the absence of transcription [8, 60].

In agreement with the literature, the LD number showed a shorter period (16 h) after CHIR99021 treatment than the 29-h oscillation in control cultures [59, 60]. Overall, the content of LDs in CHIR9901-treated cells showed a marked decrease by 36 h after synchronization with a damping amplitude compared to the controls.

On the other hand, no significant variations were observed in the LD content after the genetic disruption of LIPIN-1 over the evaluated times. A possible explanation for this result is that during LIPIN-1 downregulation LD content remained unaltered by the upregulation of LIPIN2 or through exacerbated deacylation/reacylation cycles [61]. LIPIN-1 is the rate-limiting enzyme for forming DAG, the precursor of GPLs and TAGs. LIPIN-1 is highly regulated by the circadian clock at the mRNA level in normal and tumor cells [15, 17] (reviewed in [3]) and its expression is strongly altered after disruption of the clock gene *Bmal1* [17]. The regulation of LIPIN-1 by the circadian clock and its role as a versatile lipid homeostasis regulator have been considered potential targets for cancer therapies [62]. Our findings highlight the circadian clock function related to the evolutionary conserved rhythmic regulation of lipid metabolism. This conservation occurs despite the differences in the LD composition of specific lipids and proteins and the different regulatory levels and mechanisms present across organisms, ranging from a simple oscillatory process in bacteria to highly complex processes in mammalian cells and likely in *C. elegans*. Moreover, in eukaryotic cells, we can infer that, as part of the cellular clock, the TTFL works together with the cytosolic kinases of the cytoscillator to regulate the temporal variations in metabolism as observed in tumor cells treated with CHIR9901 or after disruption of the molecular clock [17]. In addition, another level of regulation in the oscillations observed in the LD content of eukaryotic cells was observed after the metabolic alteration by genetic disruption of LIPIN-1 affecting levels of more complex GPLs and TAGs and turning the LD content arrhythmic or with a period longer than that in the circadian range.

The circadian control of lipid metabolism constitutes a crucial regulatory mechanism that allows organisms to optimize their energy reservoirs during the day and night to tightly adapt to environmental changes, including light/dark cycles, food availability, fasting schedules, stress and pathogen responses, and energy demands. The most ancient function described for LDs is energy storage; however, numerous novel functions are now recognized including membrane traffic and remodeling, cellular stress tolerance, metabolic regulation protein storage, and signaling pathways (reviewed in [19]). Thus, LD rhythms may also be associated with some of these processes.

Conclusion

Vital functions related to bioenergetics and lipid metabolism are common from bacteria to humans. Based on our findings, we can infer that the metabolic oscillations in LD content are conserved across different life kingdoms through a more complex mechanism from prokaryotes to eukaryotic cells (see Graphical Abstract). Our evidence in tumor cells suggests that the pharmacological modulation and the genetic disruption of the GL-synthesizing enzyme alter the LD oscillatory pattern. This highlights that the transcriptional clock and the cytosolic oscillator can operate coupled to maintain cellular homeostasis.

Supplementary Information The online version contains supplementary material available at https://doi.org/10.1007/s00018-024-05355-4.

Acknowledgements The authors are grateful to Mrs. Gabriela Schanner, Drs. Natalia Baez, Carlos Mas, Maria Cecilia Sampedro, Edgardo Buzzi and M. Florencia Fernández Delias for their excellent technical support, to Dr. César Prucca for experimental advice in the CRISPR/Cas9 editing tool, and to Dr. Maximiliano Rios for imaging procedure advice in ImageJ software.

Authors contribution All authors contributed to the study conception and design. Material preparation and data collection were performed by Paula M Wagner, Mauricio A Salgado, Ornella Turani, and Santiago J Fornasier. All authors analyzed data and results. The first draft of the manuscript was written by Paula M Wagner and Mario E Guido and all authors commented on previous versions of the manuscript. All authors read and approved the final manuscript.

Funding This work has been supported by Agencia Nacional de Promoción Científica y Técnica (FONCyT, PICT 2017-631, PICT 2020-0613 to MEG), Consejo Nacional de Investigaciones Científicas y Tecnológicas de la República Argentina (CONICET) (PIP 2014 to MEG), Secretaría de Ciencia y Tecnología de la Universidad Nacional de Córdoba (SeCyT- UNC, Consolidar 2018–2022 to MEG); Universidad Nacional del Sur Argentina (PGI 24/B298 to CB and PGI 24B292 to GAS); Agencia Nacional de Promoción Científica y Tecnológica Argentina (PICT 2017-0224 to GAS, PICT 2020-00936 to CB and PICT-2019 1590 to AS); Consejo Nacional de Investigaciones Científicas y Técnicas (CONICET) (PIP11220200102356 to CB).

Data availability The authors declare that the data supporting the findings of this study are available within the paper and its Supplementary Information files. Should any raw data files be needed in another format they are available from the corresponding author upon reasonable request.

Declarations

Conflict of interest All authors declare that they have no relevant financial or non-financial interests to disclose.

Ethical approval Not applicable.

Consent to participate Not applicable.

Consent for publication Not applicable.

References

1. Dunlap JC, Loros JJ, Decoursey PJ (2004) *Chronobiology: Biological Timekeeping*.
2. Guido ME, Garbarino-Pico E, Contin MA, Valdez DJ, Nieto PS, Verra DM, Acosta-Rodriguez VA, de Zavalía N, Rosenstein RE (2010) Inner retinal circadian clocks and non-visual photoreceptors: Novel players in the circadian system. Progress Neurobiol 92:484–504. https://doi.org/10.1016/J.PNEUROBIO.2010.08.005
3. Guido ME, Monjes NM, Wagner PM, Salvador GA (2022) Circadian regulation and clock-controlled mechanisms of glycerophospholipid metabolism from neuronal cells and tissues to fibroblasts. Mol Neurobiol 59:326–353. https://doi.org/10.1007/S12035-021-02595-4
4. Partch CL, Green CB, Takahashi JS (2014) Molecular architecture of the mammalian circadian clock. Trends Cell Biol. https://doi.org/10.1016/J.TCB.2013.07.002
5. Flanagan A, Bechtold DA, Pot GK, Johnston JD (2021) Chrononutrition: from molecular and neuronal mechanisms to human epidemiology and timed feeding patterns. J Neurochem. https://doi.org/10.1111/jnc.15246
6. Takahashi JS (2020) Transcriptional architecture of the mammalian circadian clock. Nat Rev Genet. https://doi.org/10.1038/nrg.2016.150
7. O'Neill JS, Reddy AB (2011) Circadian clocks in human red blood cells. Nature 469:498–503. https://doi.org/10.1038/nature09702
8. O'Neill JS, van Ooijen G, Dixon LE, Troein C, Corellou F, Bouget F-Y, Reddy AB, Millar AJ (2011) Circadian rhythms persist without transcription in a eukaryote. Nature. https://doi.org/10.1038/nature09654
9. Li W, Wang Z, Cao J, Dong Y, Chen Y (2023) Perfecting the life clock: the journey from PTO to TTFL. Int J Mol Sci. https://doi.org/10.3390/IJMS24032402
10. Hastings MH, Maywood ES, O'Neill JS (2008) Cellular circadian pacemaking and the role of cytosolic rhythms. Curr Biol 18:805–815. https://doi.org/10.1016/j.cub.2008.07.021
11. Edgar RS, Green EW, Zhao Y, van Ooijen G, Olmedo M, Qin X, Yao X et al (2012) Peroxiredoxins are conserved markers of circadian rhythms. Nature. https://doi.org/10.1038/nature11088
12. Ko CH, Yamada YR, Welsh DK, Buhr ED, Liu AC, Zhang EE, Ralph MR, Kay SA, Forger DB, Takahashi JS (2010) Emergence of noise-induced oscillations in the central circadian pacemaker. PLoS Biol. https://doi.org/10.1371/journal.pbio.1000513
13. Maywood ES, Chesham JE, O'Brien JA, Hastings MH (2011) A diversity of paracrine signals sustains molecular circadian cycling in suprachiasmatic nucleus circuits. Proc Natl Acad Sci USA 108:14306–14311. https://doi.org/10.1073/pnas.1101767108
14. Putker M, Wong DCS, Seinkmane E, Rzechorzek NM, Zeng A, Hoyle NP, Chesham JE et al (2021) Cryptochromes confer robustness, not rhythmicity to circadian timekeeping. EMBO J. https://doi.org/10.15252/EMBJ.2020106745
15. Wagner PM, Sosa LG, Alderete LD, Gorné VG, Salvador G, Pasquaré S, Guido ME (2018) Proliferative glioblastoma cancer cells exhibit persisting temporal control of metabolism and display differential temporal drug susceptibility in chemotherapy. Mol Neurobiol. https://doi.org/10.1007/s12035-018-1152-3
16. Wagner PM, Prucca CG, Fabiola FN, Sosa Alderete LG, Caputto BL, Guido ME (2021) Temporal regulation of tumor growth in nocturnal mammals: In vivo studies and chemotherapeutical potential. FASEB J 35:21231. https://doi.org/10.1096/fj.202001753R
17. Monjes NM, Wagner PM, Guido ME (2022) Disruption of the molecular clock severely affects lipid metabolism in a hepatocellular carcinoma cell model. J Biol Chem. https://doi.org/10.1016/J.JBC.2022.102551
18. Olzmann JA, Carvalho P (2019) Dynamics and functions of lipid droplets. Nat Rev Mol Cell Biol 20:137–155. https://doi.org/10.1038/s41580-018-0085-z
19. Lundquist PK, Shivaiah K-K, Espinoza-Corral R (2020) Lipid droplets throughout the evolutionary tree. Progress Lipid Res. https://doi.org/10.1016/j.plipres.2020.101029
20. Roberts MA, Olzmann JA (2020) Protein quality control and lipid droplet metabolism. Annu Rev Cell Dev Biol. https://doi.org/10.1146/ANNUREV-CELLBIO-031320-101827
21. Bermúdez MA, Balboa MA, Balsinde J (2021) Lipid droplets, phospholipase A2, arachidonic acid, and atherosclerosis. Biomedicines. https://doi.org/10.3390/BIOMEDICINES9121891
22. Zhang W, Linyong X, Zhu L, Liu Y, Yang S, Zhao M (2021) Lipid droplets, the central hub integrating cell metabolism and the immune system. Front Physiol. https://doi.org/10.3389/FPHYS.2021.746749
23. Rinia HA, Burger KNJ, Bonn M, Müller M (2008) Quantitative label-free imaging of lipid composition and packing of individual cellular lipid droplets using multiplex CARS microscopy. Biophys J 95:4908–4914. https://doi.org/10.1529/BIOPHYSJ.108.137737
24. Gooley JJ (2016) Circadian regulation of lipid metabolism. Proc Nutr Soc. https://doi.org/10.1017/S0029665116000288
25. Luján AM, Sofía F, Smania AM (2017) Draft genome sequence of pseudomonas aeruginosa strain Hex1T isolated from soils contaminated with used lubricating oil in argentina. Genome Announc. https://doi.org/10.1128/genomeA.01473-16
26. Turani O, Hernando G, Corradi J, Bouzat C (2018) Activation of caenorhabditis elegans levamisole-sensitive and mammalian nicotinic receptors by the antiparasitic bephenium. Mol Pharmacol 94:1270–1279. https://doi.org/10.1124/MOL.118.113357
27. Hernando G, Turani O, Bouzat C (2019) Caenorhabditis elegans muscle Cys-loop receptors as novel targets of terpenoids with

potential anthelmintic activity. PLoS. https://doi.org/10.1371/JOURNAL.PNTD.0007895
28. van der Linden AM, Beverly M, Kadener S, Rodriguez J, Wasserman S, Rosbash M, Sengupta P (2010) Genome-wide analysis of light- and temperature-entrained circadian transcripts in caenorhabditis elegans. PLOS Biol 8:e1000503
29. Balsalobre A, Damiola F, Schibler U (1998) A serum shock induces circadian gene expression in mammalian tissue culture cells. Cell 93:929–937
30. Porras MA, Villar MA, Cubitto MA (2017) Novel spectrophotometric technique for rapid determination of extractable PHA using Sudan black dye. J Biotechnol. https://doi.org/10.1016/J.JBIOTEC.2017.06.012
31. Porras MA, Villar MA, Cubitto MA (2018) Improved intracellular PHA determinations with novel spectrophotometric quantification methodologies based on Sudan black dye. J Microbiol Methods 148:1–11. https://doi.org/10.1016/J.MIMET.2018.03.008
32. Wang FY, Ching TT (2021) Oil red O staining for lipid content in caenorhabditis elegans. Bio-Protoc. https://doi.org/10.21769/BIOPROTOC.4124
33. Yue Y, Li S, Shen P, Park Y (2021) Caenorhabditis elegans as a model for obesity research. Curr Res Food Sci 4:692–697. https://doi.org/10.1016/J.CRFS.2021.09.008
34. Cheng X, Geng F, Pan M, Xiaoning W, Zhong Y, Wang C, Tian Z et al (2020) Targeting DGAT1 ameliorates glioblastoma by increasing fat catabolism and oxidative stress. Cell Metab. https://doi.org/10.1016/J.CMET.2020.06.002
35. Wu G, Anafi RC, Hughes ME, Kornacker K, Hogenesch JB (2016) MetaCycle: an integrated R package to evaluate periodicity in large scale data. Bioinformatics. https://doi.org/10.1093/bioinformatics/btw405
36. Thaben PF, Westermark PO (2014) Detecting rhythms in time series with RAIN. J Biol Rhythms 29:391–400. https://doi.org/10.1177/0748730414553029
37. Acosta-Rodríguez V, Rijo-Ferreira F, Izumo M, Pin X, Wight-Carter M, Green CB, Takahashi JS (2022) Circadian alignment of early onset caloric restriction promotes longevity in male C57BL/6J mice. Science 376:1192–1202
38. Zhang SO, Box A, Ningyi X, Le Men J, Jingyi Y, Guo F, Trimble R, Mak HY (2010) Genetic and dietary regulation of lipid droplet expansion in Caenorhabditis elegans. Proc Natl Acad Sci USA 107:4640. https://doi.org/10.1073/PNAS.0912308107
39. Goya ME, Romanowski A, Caldart CS, Bénard CY, Golombek DA (2016) Circadian rhythms identified in Caenorhabditis elegans by in vivo long-term monitoring of a bioluminescent reporter. Proc Natl Acad Sci USA 113:E7837–E7845. https://doi.org/10.1073/PNAS.1605769113
40. Escorcia W, Ruter DL, Nhan J, Curran SP (2018) Quantification of lipid abundance and evaluation of lipid distribution in caenorhabditis elegans by nile red and Oil red O staining. J Vis Exp. https://doi.org/10.3791/57352
41. O'Rourke EJ, Soukas AA, Carr CE, Ruvkun G (2009) C. elegans major fats are stored in vesicles distinct from lysosome-related organelles. Cell Metab 10:430–435. https://doi.org/10.1016/J.CMET.2009.10.002
42. Wagner PM, Monjes NM, Guido ME (2019) Chemotherapeutic effect of SR9009, a REV-ERB agonist, on the human glioblastoma T98G cells. ASN Neuro 11:175909141989271. https://doi.org/10.1177/1759091419892713
43. Danielli M, Perne L, Jovičić EJ, Petan T (2023) Lipid droplets and polyunsaturated fatty acid trafficking. Balancing Life Death. https://doi.org/10.3389/fcell.2023.1104725
44. Lasker K (2022) Mesoscale organization in bacteria. Nat Rev Mol Cell Biol 23:230–230. https://doi.org/10.1038/s41580-022-00459-w
45. Bar-Peled L, Kory N (2022) Principles and functions of metabolic compartmentalization. Nat Metab 4:1232. https://doi.org/10.1038/S42255-022-00645-2
46. Alvarez HM (2015) Triacylglycerol and wax ester-accumulating machinery in prokaryotes. Biochimie. https://doi.org/10.1016/j.biochi.2015.08.016
47. Wältermann M, Hinz A, Robenek H, Troyer D, Reichelt R, Malkus U, Galla HJ et al (2005) Mechanism of lipid-body formation in prokaryotes: how bacteria fatten up. Mol Microbiol 55:750–763. https://doi.org/10.1111/J.1365-2958.2004.04441.X
48. Hernández MA, Mohn WW, Martínez E, Rost E, Alvarez AF, Alvarez HM (2008) Biosynthesis of storage compounds by Rhodococcus jostii RHA1 and global identification of genes involved in their metabolism. BMC Genomics 9:1–14. https://doi.org/10.1186/1471-2164-9-600/FIGURES/6
49. Jendrossek D (2009) Polyhydroxyalkanoate granules are complex subcellular organelles (Carbonosomes). J Bacteriol 191:3195. https://doi.org/10.1128/JB.01723-08
50. Sengupta P, Garrity P (2013) Sensing temperature. Curr Biol 23:R304–R307. https://doi.org/10.1016/J.CUB.2013.03.009
51. Almblad H, Randall TE, Liu F, Leblanc K, Groves RA, Kittichotirat W, Winsor GL et al (2021) Bacterial cyclic diguanylate signaling networks sense temperature. Nat Commun 12:1–14. https://doi.org/10.1038/s41467-021-22176-2
52. Kahl LJ, Eckartt KN, Morales DK, Price-Whelan A (2022) Light/Dark and temperature cycling modulate metabolic electron flow in pseudomonas aeruginosa biofilms. MBio. https://doi.org/10.1128/MBIO.01407-22/SUPPL_FILE/MBIO.01407-22-S0009.TXT
53. Zhang SO, Trimble R, Guo F, Mak HY (2010) Lipid droplets as ubiquitous fat storage organelles in C. elegans. BMC Cell Biol 11:96. https://doi.org/10.1186/1471-2121-11-96
54. Migliori ML, Goya ME, Lamberti ML, Silva F, Rota R, Bénard C, Golombek DA (2023) Caenorhabditis elegans as a promising model organism in chronobiology. J Biol Rhythms 38:131–147. https://doi.org/10.1177/07487304221143483
55. Huang E, Cheng S-Y, Kou Y, Geng F, Guo D (2022) Lipid metabolism in glioblastoma: from de novo synthesis to storage. Biomedicines. https://doi.org/10.3390/biomedicines
56. Tauchi-Sato K, Ozeki S, Houjou T, Taguchi R, Fujimoto T (2002) The surface of lipid droplets is a phospholipid monolayer with a unique fatty acid composition. J Biol Chem 277:44507–44512. https://doi.org/10.1074/JBC.M207712200
57. Gréchez-Cassiau A, Feillet C, Guérin S, Delaunay F (2015) The hepatic circadian clock regulates the choline kinase α gene through the BMAL1-REV-ERBα axis. Chronobiol Int 32:774–784. https://doi.org/10.3109/07420528.2015.1046601
58. Liu R, Lee JH, Li J, Yu R, Tan K, Xia Y, Zheng Y (2021) Choline kinase alpha 2 acts as a protein kinase to promote lipolysis of lipid droplets. Mol Cell 81:2722–2735
59. Causton HC, Feeney KA, Ziegler CA, O'Neill JS (2015) Metabolic cycles in yeast share features conserved among circadian rhythms. Curr Biol 25:1056–1062. https://doi.org/10.1016/j.cub.2015.02.035
60. Hirota T, Lewis WG, Liu AC, Jae WL, Schultz PG, Kay SA (2008) A chemical biology approach reveals period shortening of the mammalian circadian clock by specific inhibition of GSK-3β. Proc Natl Acad Sci USA 105:20746. https://doi.org/10.1073/PNAS.0811410106
61. Dwyer JR, Donkor J, Zhang P, Csaki LS, Vergnes L, Lee JM, Dewald J et al (2012) Mouse lipin-1 and lipin-2 cooperate to maintain glycerolipid homeostasis in liver and aging cerebellum. Proc Natl Acad Sci USA 109:2486. https://doi.org/10.1073/PNAS.1205221109/-/DCSUPPLEMENTAL
62. Brohée L, Crémer J, Colige A, Deroanne C (2021) Lipin-1, a versatile regulator of lipid homeostasis, is a potential target for fighting cancer. Int J Mol Sci. https://doi.org/10.3390/IJMS22094419

Authors and Affiliations

Paula M. Wagner[1,2] · Mauricio A. Salgado[1,2] · Ornella Turani[3] · Santiago J. Fornasier[1,2] · Gabriela A. Salvador[3] · Andrea M. Smania[1,2] · Cecilia Bouzat[3] · Mario E. Guido[1,2]

✉ Mario E. Guido
mario.guido@unc.edu.ar

[1] CIQUIBIC-CONICET, Facultad de Ciencias Químicas, Universidad Nacional de Córdoba, 5000 Córdoba, Argentina

[2] Departamento de Química Biológica Ranwel Caputto, Facultad de Ciencias Químicas, Universidad Nacional de Córdoba, Haya de la Torre s/n, Ciudad Universitaria, 5000 Córdoba, Argentina

[3] INIBIBB-CONICET, Universidad Nacional del Sur, Departamento de Biología, Bioquímica y Farmacia, Camino de la Carrindanga, km 7, 8000 Bahía Blanca, Argentina